prepared protein extracts were quantified using a Protein Assay kit (Bio-Rad, Hercules, CA), which is based on the Bradford method. Aliquots were separated by 4–20% sodium dodecyl sulfate polyacrylamide gel electrophoresis (SDS–PAGE) and transferred to polyvinylidene difluoride microporous membranes (GE Healthcare Bio-Science, Piscataway, NJ) using a semi-dry blotter. The membranes were then incubated with the primary antibodies described above for 1 hr at room temperature, followed by incubation with peroxidase-conjugated secondary antibodies for 40 min at room temperature. The bound antibodies were visualized using an ECL kit (GE Healthcare Bio-Science) and the membranes were exposed to X-ray film (GE Healthcare Bio-Science).

RNA Isolation, ReverseTranscription and Quantitative Real-Time Polymerase Chain Reaction (PCR)

RNA isolation and reverse transcription were performed as described previously [10–12,14]. Quantitative real-time PCR was performed using TaqMan Gene Expression Assays for *Twist1* (Hs00361186_m1), *YB-1* (Hs00898625_g1), *AR* (Hs00907244_m1), and *glyceraldehyde-3-phosphate dehydrogenase* (*GAPDH*; Hs02758991_g1) (Applied Biosystems, Foster City, CA) and TaqMan Gene Expression Master Mix (Applied Biosystems) on a 7900HT PCR system (Applied Biosystems). The transcript levels of *Twist1*, *YB-1*, and *AR* were corrected with reference to the corresponding *GAPDH* transcript levels. All values represent the results of at least three independent experiments.

Cytotoxicity Analysis

Cytotoxicity analyses were performed as described previously [14]. Briefly, prostate cancer cells (2.5×10^3) were seeded in 96-well plates. On the following day, various concentrations of drugs were applied. After 48 hr, the surviving cells were stained using the alamarBlue assay (TREK Diagnostic Systems, Cleveland, OH) at 37°C for 3 hr. The absorbance of each well was measured using an ARVO™ MX plate reader (Perkin Elmer, Inc., Waltham, MA). The results were representative of at least three independent experiments.

Cell Proliferation Assay

Cell proliferation assays were performed as described previously [10,11,14]. Briefly, prostate cancer cells (2.5×10^4) were seeded into 12-well plates and incubated in medium containing 10% FBS or charcoal-stripped serum (CSS). After 96 hr, cells were harvested with trypsin and counted using a cell counter (Beckman Coulter, Fullerton, CA). The results were normalized to cell counts at 0 hr and were representative of three experiments.

RESULTS

Hydrogen Peroxide-Resistant Cells and Castration-Resistant Cells Are Cross-Resistant to Hydrogen Peroxide and Anticancer Drugs

Cancer cells are known to acquire a multi-drug resistant phenotype during exposure to several anticancer drugs [6]. We examined cellular resistance to anticancer drugs in hydrogen peroxide-resistant LNCaP cells (HPR50 cells). As expected, hydrogen peroxide-resistant cells were cross-resistant to docetaxel and cisplatin, as well as to hydrogen peroxide, but not to 5-fluorouracil (5-FU; Fig. 1A). Because HPR50 cells were resistant to castration, similar to castration-resistant LNCaP cells (CxR cells), we next

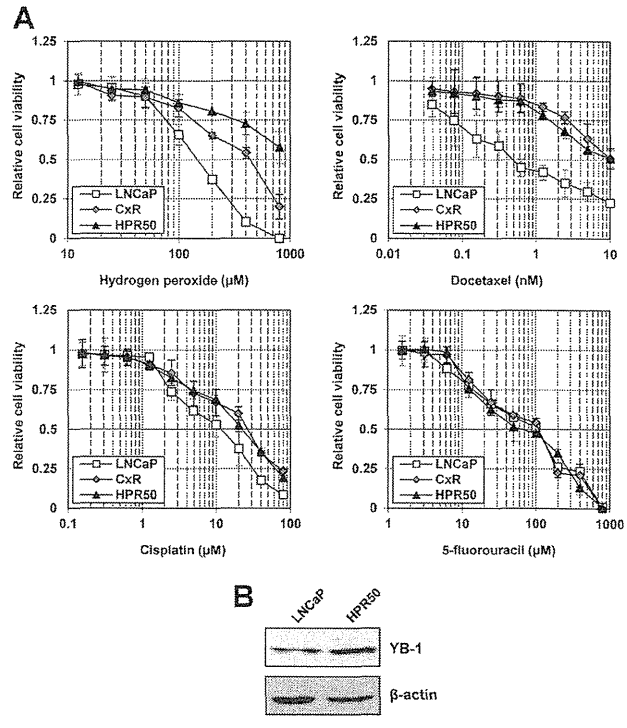

Fig. 1. Hydrogen peroxide-resistant cells and castration-resistant cells are cross-resistant to hydrogen peroxide and anticancer drugs. **A**: LNCaP, CxR, and HRP50 cells were seeded in 96-well plates. On the following day, various concentrations of hydrogen peroxide, docetaxel, cisplatin, and 5-FU were applied. After 48 hr, the cell survival rates were analyzed by cytotoxicity analyses. Cell survival in the absence of drugs was defined as one. The data shown are mean ± SD. **B**: Whole-cell extracts from LNCaP and HPR50 cells were subjected to SDS–PAGE, followed by Western blotting analyses of the indicated proteins.

examined cellular sensitivity to anticancer agents using CxR cells. CxR cells were also resistant to hydrogen peroxide, docetaxel, and cisplatin, but not to 5-FU, as seen in HPR50 cells (Fig. 1A).

We found previously that both Twist1 and YB-1 were up-regulated in CxR cells compared with LNCaP cells, and that Twist1 was overexpressed in HPR50 cells [10,11]. Similarly, YB-1 expression was increased in HPR50 cells (Fig. 1B), suggesting a close link between Twist1 and YB-1 in these resistant cells.

Transforming-Growth Factor-β (TGF-β) Induces Twist1 and YB-1 Expression in Prostate Cancer Cells

We previously showed that Twist1 knockdown using Twist1-specific siRNAs reduced *YB-1* mRNA expression in LNCaP cells [10]. Similarly, Twist1 knockdown decreased *YB-1* transcript level in PC-3 cells (Fig. 2A). Conversely, Twist1 overexpression by an expression plasmid induced *YB-1* transcription, represented by increased *YB-1* mRNA levels after Twist1 overexpression in both LNCaP and PC-3 cells (Fig. 2B).

To confirm the relationship between Twist1 and YB-1 expression, we used the taxane-resistance factor TGF-β [15] (which is a known inducer of Twist1 in epithelial–mesenchymal transition) in PC-3 cells expressing the TGF-β receptor. TGF-β induced expression of *Twist1* as well as *YB-1* at the mRNA (Fig. 3A,B) and protein levels (Fig. 3C,D), suggesting a close functional link among TGF-β, Twist1, and YB-1 in taxane resistance.

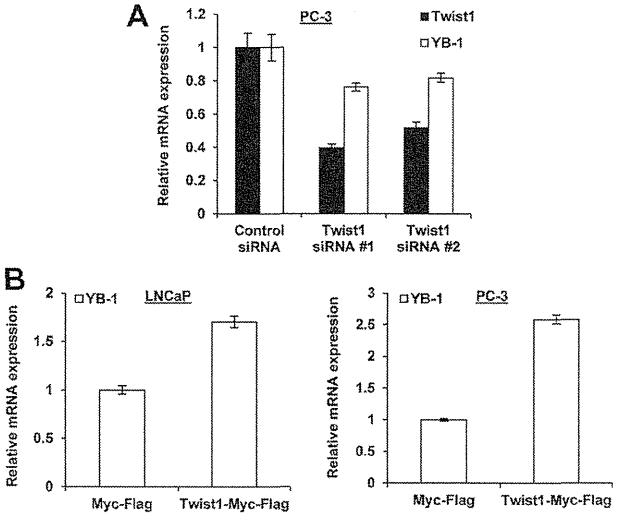

Fig. 2. Twist1 regulates YB-1 expression in prostate cancer cells. **A**: PC-3 cells were transfected with 40 nM of the indicated siRNA and incubated for 48 hr. After extraction of total RNA and synthesis of cDNA, quantitative real-time PCR was performed for *Twist1*, *YB-1*, and *GAPDH*. Each target transcript level was corrected relative to the corresponding *GAPDH* transcript level. The level of each target transcript in cells transfected with the control siRNA was defined as one. The data shown are mean ± SD. **B**: LNCaP and PC-3 cells were transfected with 1.0 μg/ml of the indicated plasmid and incubated for 48 hr. After extraction of total RNA and synthesis of cDNA, quantitative real-time PCR was performed for *YB-1* and *GAPDH*. Each target transcript level was corrected relative to the corresponding *GAPDH* transcript level. The level of each target transcript in cells transfected with the mock plasmid (Myc-Flag) was defined as one. The data shown are mean ± SD.

Twist1 and YB-1 Are Activated in Docetaxel-Resistant Cells

To reveal the roles of Twist1 and YB-1 in cellular resistance to docetaxel, we investigated their statuses in docetaxel-resistant cell lines. We established docetaxel-resistant cell lines from PC-3, DU145, and LNCaP

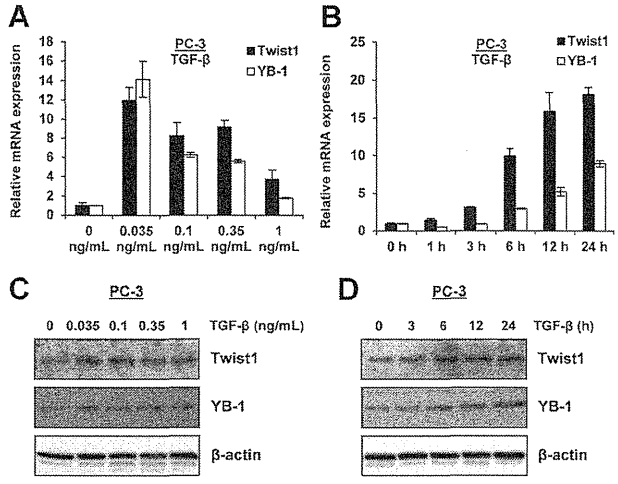

Fig. 3. TGF-β induces Twist1 as well as YB-1 expression in PC-3 cells. **A**: PC-3 cells were treated with the indicated concentration of TGF-β for 24 hr. After extraction of total RNA and synthesis of cDNA, quantitative real-time PCR was performed for *Twist1*, *YB-1*, and *GAPDH*. Each target transcript level was corrected relative to the corresponding *GAPDH* transcript level. The level of each target transcript in PC-3 cells treated with vehicle was defined as one. The data shown are mean ± SD. **B**: PC-3 cells were treated with 1 ng/ml of TGF-β for the indicated duration. After extraction of total RNA and synthesis of cDNA, quantitative real-time PCR was performed for *Twist1*, *YB-1*, and *GAPDH*. Each target transcript level was corrected relative to the corresponding *GAPDH* transcript level. The level of each target transcript in PC-3 cells treated with vehicle was defined as one. The data shown are mean ± SD. **C**: PC-3 cells were treated with the indicated concentration of TGF-β for 24 hr. Whole-cell extracts were subjected to SDS–PAGE, followed by Western blotting analyses for the indicated proteins. **D**: PC-3 cells were treated with 1 ng/ml of TGF-β for the indicated duration. Whole-cell extracts were subjected to SDS–PAGE, followed by Western blotting analyses for the indicated proteins.

cells. Their sensitivities to docetaxel were twofold to threefold lower in docetaxel-resistant cells compared with their parental cells (Fig. 4A). We examined the statuses of Twist1 and YB-1 in these docetaxel-resistant cells. Twist1 expression was increased in docetaxel-resistant PC-3 cells (PC-3/DTX), as well as in docetaxel-resistant LNCaP cells (LNCaP/DTX), though parental DU145 and docetaxel-resistant DU145 (DU145/DTX) cells did not express Twist1 protein. Similarly, phosphorylated YB-1, representing activated YB-1, was increased in docetaxel-resistant DU145 cells (DU145/DTX) and LNCaP/DTX cells (Fig. 4B), which was compatible with our finding that total YB-1 expression was augmented in DU145/DTX and LNCaP/DTX cells [8]. Furthermore, docetaxel treatment induced activation of YB-1, but not Twist1 or total YB-1 expression (Fig. 4C).

Reducing Twist1 and YB-1 as Well as AR Expression Sensitizes LNCaP Cells to Docetaxel

To reveal the relevance of Twist1 and YB-1, we examined the cellular sensitivities to anticancer drugs after Twist1 or YB-1 knockdown. Twist1 and YB-1 knockdown sensitized LNCaP cells to docetaxel and cisplatin (Fig. 5A,B). In addition, reducing Twist 1 and YB-1 expression increased cellular sensitivity to hydrogen peroxide (Fig. 5C), but not to 5-FU (Fig. 5D).

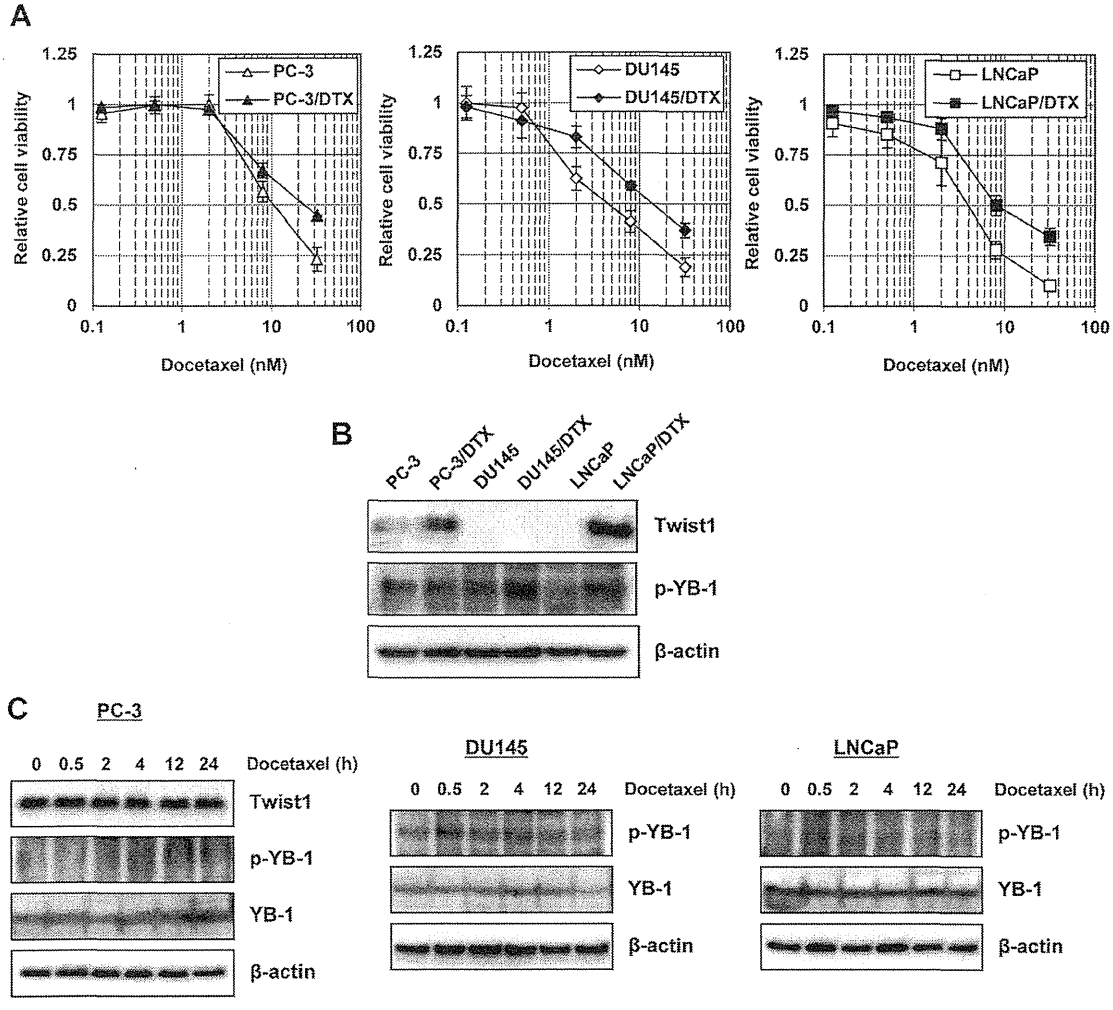

Fig. 4. Twist1 and YB1 are activated in docetaxelresistant cells. **A**: The indicated cells were seeded in 96well plates. On the following day, various concentrations of docetaxel were applied. After 48 hr, the cell survival rates were analyzed by cytotoxicity analyses. Cell survival in the absence of docetaxel was defined as one. The data shown are mean . . SD. **B**: Wholecell extracts from the indicated cells were subjected to SDSPAGE, followed by Western blotting analyses for the indicated proteins. **C**: PC3, DU145, and LNCaP cells were treated with 2.5 nM of docetaxel for the indicated duration. Wholecell extracts were subjected to SDSPAGE, followed by Western blotting analyses for the indicated proteins.

We showed previously that both Twist1 and YB-1 promoted AR expression in LNCaP cells [10,11]. We investigated the role of AR in cellular resistance to anticancer drugs by comparing AR expression levels between LNCaP and LNCaP/DTX cells. Unexpectedly, AR expression was decreased in LNCaP/DTX cells compared with LNCaP cells at both transcript and protein levels (Fig. 6A). However, AR knockdown rendered LNCaP cells sensitive to docetaxel and hydrogen peroxide, but not to cisplatin and 5-FU (Fig. 6B). In addition, growth of LNCaP/DTX cells was effectively suppressed under androgen-deprived conditions, compared with that of LNCaP cells (Fig. 6C).

DISCUSSION

The results of this study revealed that hydrogen peroxide-resistant and CRPC cells are cross-resistant to anticancer drugs, including cisplatin and docetaxel, in addition to hydrogen peroxide. However, cellular sensitivity to 5-FU was constant, which was compatible with a previous report indicating that Twist1, YB-1 and AR were not involved in cellular resistance to 5-FU [5,14]. Kosaka et al. [16] recently reported that C4-2 cells incubated under androgen-depleted condition were cross-resistant to docetaxel, accompanied by increased phosphorylation of Akt. In addition, over-

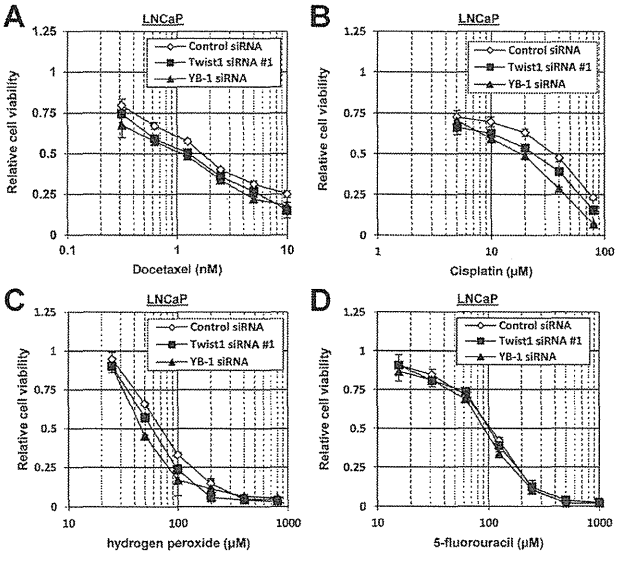

Fig. 5. Twist1 and YB-1 knockdown modulates cellular sensitivity to docetaxel, cisplatin and hydrogen peroxide, but not to 5-FU. **A–D**: LNCaP cells were transfected with 40 nM of the indicated siRNA and seeded in 96-well plates. On the following day, various concentrations of docetaxel (A), cisplatin (B), hydrogen peroxide (C), and 5-FU (D) were applied. After 48 hr, the cell survival rates were analyzed by cytotoxicity analyses. Cell survival in the absence of drugs was defined as one. The data shown are mean ± SD.

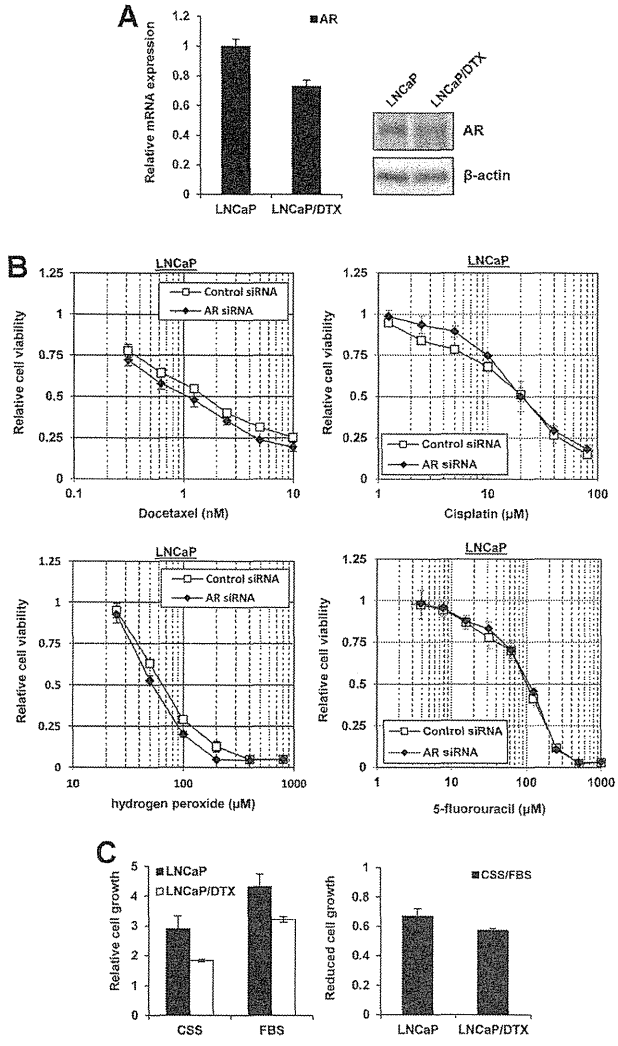

Fig. 6. AR knockdown modulates cellular sensitivity to docetaxel and hydrogen peroxide, but not to cisplatin and 5-FU. **A**: After extraction of total RNA from LNCaP and LNCaP/DTX cells and synthesis of cDNA, quantitative real-time PCR was performed for *AR* and *GAPDH*. Each target transcript level was corrected relative to the corresponding *GAPDH* transcript level. The level of each target transcript in LNCaP cells was defined as one. The data shown are mean ± SD. Whole-cell extracts from LNCaP and LNCaP/DTX cells were subjected to SDS–PAGE, followed by Western blotting analyses for the indicated proteins. **B**: LNCaP cells were transfected with 40 nM of the indicated siRNA and seeded in 96-well plates. On the following day, various concentrations of docetaxel, cisplatin, hydrogen peroxide and 5-FU were applied. After 48 hr, the cell survival rates were analyzed by cytotoxicity analyses. Cell survival in the absence of drugs was defined as one. The data shown are mean ± SD. **C**: LNCaP and LNCaP/DTX cells were seeded and incubated in medium with 10% FBS and CSS. The number of cells was counted at 96 hr. The results were normalized to the number of cells at 0 hr. All values represent at least three independent experiments. The data shown are mean ± SD.

expression of the taxane-resistance factors P-gp, βIII-tubulin, and clusterin in CRPC suggests that CRPC is cross-resistant to docetaxel through these taxane-resistant factors [7,8,17]. These data suggest that a common pathway including Akt, P-gp, βIII-tubulin, and clusterin is involved in both castration resistance and taxane resistance.

Several factors including P-gp, βIII-tubulin, and clusterin are known to be involved in taxane resistance. YB-1 is thought to promote taxane resistance via expression of P-gp and clusterin [7,8]. Similarly, Twist1 is also known to augment taxane resistance [4,5]. Furthermore, TGF-β as an inducer of Twist1 and YB-1 expression is also known to play a role in promoting taxane resistance, suggesting that TGF-β/Twist1/YB-1 signaling at least in PC-3 cells contributes to taxane resistance in addition to epithelial–mesenchymal transition [15]. This study also showed that both Twist1 and YB-1 were involved in cellular sensitivity to hydrogen peroxide. Intriguingly, the transcriptional activities of both YB-1 and Twist1 were modulated by oxidative stress. Classically, hydrogen peroxide induced activation of YB-1, leading to MHC class II *HLA-DQ* gene expression [6]. In addition, hydrogen peroxide was recently identified as a potent inducer of YB-1 accumulation by the calcineurin inhibitor cyclosporine A [18]. Similarly, oxidative stress caused by hydrogen peroxide induced Twist1 expression [10], as well as modulating Twist1 dimerization from a Twist1 homodimer to a Twist1-E2a heterodimer [19], leading to induction of Twist1 transactivation. Activation of YB-1 and Twist1 by oxidative stress may thus play a protective role in oxidative stress. Furthermore, the similar drug-resistance characteristics of Twist1 and YB-1 appear to represent a functional link between Twist1 and YB-1, as indicated by the demonstration of mutual regulation of Twist1 and YB-1 in current and previous studies [5,9]. In addition to contributions to taxane resistance by both Twist1 and YB-1, AR was also shown to be involved in taxane resistance. Intriguingly, androgen regulates expression of the taxane resistance-promoting factor βIII-tubulin [20,21] suggesting that AR reactivation in CRPC may contribute to taxane resistance via βIII-tubulin up-regulation, which is supported by the finding that βIII-tubulin expression was increased in CRPC [17]. Because Twist1 and YB-1 regulate AR expression [10,11], their contributions to taxane resistance may, at least partially, be associated with AR signaling. Taken together, taxane resistance in CRPC may be the result of activation of Twist1/YB-1 signaling, as well as AR activation.

However, AR expression in docetaxel-resistant LNCaP cells was decreased compared with parental cells, though Twist1 and/or YB-1 were activated. Taxanes were reported to inhibit AR expression [22], nuclear translocation of AR [23,24], and transactivation of AR [25], independently of Twist1 and YB-1. AR down-regulation in docetaxel-resistant cells may thus be a result of exposure to docetaxel itself. AR expression is known to be a critical factor for cell sensitivity to castration. In fact, docetaxel-resistant LNCaP cells expressing lower levels of ARs were sensitive to androgen deprivation, suggesting that initial taxane treatment before ADT may be more effective than salvage taxane treatment after androgen deprivation. Several studies to date have suggested that taxane treatment is effective against hormone-naïve prostate cancer. A preclinical study showed that concurrent therapy using paclitaxel and androgen deprivation produced better tumor control than sequential therapy using paclitaxel and androgen deprivation in Shionogi and LNCaP tumor models [26]. Intriguingly, this study also showed superior initial suppression of LNCaP tumor growth by sequential therapy using paclitaxel prior to androgen deprivation, compared with androgen deprivation followed by paclitaxel, which is the current standard therapy [26], suggesting the possible superiority of taxane treatment prior to ADT. In a phase II clinical study, neoadjuvant docetaxel and ADT was associated with encouraging recurrence-free survival [27]. In addition, docetaxel alone showed a durable prostate-specific antigen (PSA) decline of >50% in 43% of hormone-naïve prostate cancer patients who relapsed after surgery and/or radiation [28]. Similarly, docetaxel plus estramustine reduced PSA to below detection levels in 53%, and resulted in a 90% PSA decline in 81% of patients with relapsed prostate cancer after prostatectomy and/or radiation [29]. Moreover, in a retrospective study, combination chemotherapy including docetaxel effectively reduced PSA and improved overall survival in 31 hormone-naïve patients with locally advanced or metastatic prostate cancer [30]. These results suggest that initial taxane treatment before or concurrent with ADT may confer a therapeutic benefit in patients with recurrent or advanced prostate cancer, especially with high risk of becoming refractory to ADT.

CONCLUSIONS

The Twist1/YB-1 pathway, as well as AR, is activated in CRPC cells and contributes to multi-drug resistance, including taxane resistance. However, ARs are down-regulated in docetaxel-resistant prostate cancer cells, and appear to confer a successful therapeutic effect of androgen deprivation in prostate cancer cells. Overall, these findings suggest that initial taxane treatment of hormone-naïve prostate cancer patients may be more effective than salvage taxane

treatment after androgen-deprivation therapy in CRPC, which is the current therapeutic sequence for patients with recurrent or advanced prostate cancer. This study therefore demonstrates the rationale of primary taxane treatment of hormone-naïve prostate cancer and suggests that further prospective clinical trials are justified to compare the relative benefits of taxanes with or without androgen deprivation for hormone-naïve prostate cancer.

ACKNOWLEDGMENTS

We would like to thank Dr. Dongchon Kang (Kyushu University, Fukuoka, Japan) for assistance with the quantitative real-time PCR, Edanz Group Japan for editorial assistance, and Ms. Noriko Hakoda and Ms. Eriko Gunshima for technical assistance. This work was supported by Kakenhi grants (22591769 to A.Y. and 24890160 to M.S.) from the Ministry of Education, Culture, Sports, Science and Technology of Japan (MEXT), Japan, a Medical Research Promotion Grant from Takeda Science Foundation to MS, Japan, and a Research Promotion Grant from the Uehara Memorial Foundation to MS, Japan.

REFERENCES

1. Tannock IF, de Wit R, Berry WR, Horti J, Pluzanska A, Chi KN, Oudard S, Théodore C, James ND, Turesson I, Rosenthal MA, Eisenberger MA, TAX 327 Investigators. Docetaxel plus prednisone or mitoxantrone plus prednisone for advanced prostate cancer. N Engl J Med 2004;351(15):1502–1512.
2. de Bono JS, Oudard S, Ozguroglu M, Hansen S, Machiels JP, Kocak I, Gravis G, Bodrogi I, Mackenzie MJ, Shen L, Roessner M, Gupta S. Sartor AO, TROPIC Investigators. Prednisone plus cabazitaxel or mitoxantrone for metastatic castration-resistant prostate cancer progressing after docetaxel treatment: A randomised open-label trial. Lancet 2010;376(9747):1147–1154.
3. Fujimoto N, Shiota M, Kubo T, Matsumoto T. Novel therapeutic strategies following docetaxel-based chemotherapy in castration-resistant prostate cancer. Expert Rev Clin Pharmacol 2010;3 (6):785–795.
4. Kwok WK, Ling MT, Lee TW, Lau TC, Zhou C, Zhang X, Chua CW, Chan KW, Chan FL, Glackin C, Wong YC, Wang X. Up-regulation of TWIST in prostate cancer and its implication as a therapeutic target. Cancer Res 2005;65(12):5153–5162.
5. Shiota M, Izumi H, Tanimoto A, Takahashi M, Miyamoto N, Kashiwagi E, Kidani A, Hirano G, Masubuchi D, Fukunaka Y, Yasuniwa Y, Naito S, Nishizawa S, Sasaguri Y, Kohno K. Programmed cell death protein 4 down-regulates Y-box binding protein-1 expression via a direct interaction with Twist1 to suppress cancer cell growth. Cancer Res 2009;69(7):3148–3156.
6. Kuwano M, Oda Y, Izumi H, Yang SJ, Uchiumi T, Iwamoto Y, Toi M, Fujii T, Yamana H, Kinoshita H, Kamura T, Tsuneyoshi M, Yasumoto K, Kohno K. The role of nuclear Y-box binding protein 1 as a global marker in drug resistance. Mol Cancer Ther 2004;3 (11):1485–1492.
7. Giménez-Bonafé P, Fedoruk MN, Whitmore TG, Akbari M, Ralph JL, Ettinger S, Gleave ME, Nelson CC. YB-1 is upregulated during prostate cancer tumor progression and increases P-glycoprotein activity. Prostate 2004;59(3):337–349.
8. Shiota M, Zoubeidi A, Kumano M, Beraldi E, Naito S, Nelson CC, Sorensen PH, Gleave ME. Clusterin is a critical downstream mediator of stress-induced YB-1 transactivation in prostate cancer. Mol Cancer Res 2011;9(12):1755–1766.
9. Evdokimova V, Tognon C, Ng T, Ruzanov P, Melnyk N, Fink D, Sorokin A, Ovchinnikov LP, Davicioni E, Triche TJ, Sorensen PH. Translational activation of snail1 and other developmentally regulated transcription factors by YB-1 promotes an epithelial-mesenchymal transition. Cancer Cell 2009;15(5):402–415.
10. Shiota M, Yokomizo A, Tada Y, Inokuchi J, Kashiwagi E, Masubuchi D, Eto M, Uchiumi T, Naito S. Castration resistance of prostate cancer cells caused by castration-induced oxidative stress through Twist1 and androgen receptor overexpression. Oncogene 2010;29(2):237–250.
11. Shiota M, Takeuchi A, Song Y, Yokomizo A, Kashiwagi E, Uchiumi T, Kuroiwa K, Tatsugami K, Fujimoto N, Oda Y, Naito S. Y-box binding protein-1 promotes castration-resistant prostate cancer growth via androgen receptor expression. Endocr Relat Cancer 2011;18(4):505–517.
12. Shiota M, Song Y, Takeuchi A, Yokomizo A, Kashiwagi E, Kuroiwa K, Tatsugami K, Uchiumi T, Oda Y, Naito S. Antioxidant therapy alleviates oxidative stress by androgen deprivation and prevents conversion from androgen dependent to castration resistant prostate cancer. J Urol 2012;187(2):707–714.
13. Wu CT, Chen WC, Liao SK, Hsu CL, Lee KD, Chen MF. The radiation response of hormone-resistant prostate cancer induced by long-term hormone therapy. Endocr Relat Cancer 2007;14 (3):633–643.
14. Shiota M, Takeuchi A, Yokomizo A, Kashiwagi E, Tatsugami K, Naito S. Androgen receptor signaling regulates cell growth and vulnerability to doxorubicin in bladder cancer. J Urol 2012;188 (1):276–286.
15. Marin-Aguilera M, Codony-Servat J, Kalko SG, Fernández PL, Bermudo R, Buxo E, Ribal MJ, Gascón P, Mellado B. Identification of docetaxel resistance genes in castration-resistant prostate cancer. Mol Cancer Ther 2012;11(2):329–339.
16. Kosaka T, Miyajima A, Shirotake S, Suzuki E, Kikuchi E, Oya M. Long-term androgen ablation and docetaxel up-regulate phosphorylated Akt in castration resistant prostate cancer. J Urol 2011;185(6):2376–2381.
17. Terry S, Ploussard G, Allory Y, Nicolaiew N, Boissière-Michot F, Maillé P, Kheuang L, Coppolani E, Ali A, Bibeau F, Culine S, Buttyan R, de la Taille A, Vacherot F. Increased expression of class III β-tubulin in castration-resistant human prostate cancer. Br J Cancer 2009;101(6):951–956.
18. Hanssen L, Frye BC, Ostendorf T, Alidousty C, Djudjaj S, Boor P, Rauen T, Floege J, Mertens PR, Raffetseder U. Y-box binding protein-1 mediates profibrotic effects of calcineurin inhibitors in the kidney. J Immunol 2011;187(1):298–308.
19. Danciu TE, Whitman M. Oxidative stress drives disulfide bond formation between basic helix-loop-helix transcription factors. J Cell Biochem 2010;109(2):417–424.
20. Mariani M, Zannoni GF, Sioletic S, Sieber S, Martino C, Martinelli E, Coco C, Scambia G, Shahabi S, Ferlini C. Gender influences the class III and V β-tubulin ability to predict poor outcome in colorectal cancer. Clin Cancer Res 2012;18(10):2964–2975.

21. Butler R, Leigh PN, Gallo JM. Androgen-induced up-regulation of tubulin isoforms in neuroblastoma cells. J Neurochem 2001;78 (4):854–861.

22. Kuroda K, Liu H, Kim S, Guo M, Navarro V, Bander NH. Docetaxel down-regulates the expression of androgen receptor and prostate-specific antigen but not prostate-specific membrane antigen in prostate cancer cell lines: Implications for PSA surrogacy. Prostate 2009;69(14):1579–1585.

23. Zhu ML, Horbinski CM, Garzotto M, Qian DZ, Beer TM, Kyprianou N. Tubulin-targeting chemotherapy impairs androgen receptor activity in prostate cancer. Cancer Res 2010;70 (20):7992–8002.

24. Darshan MS, Loftus MS, Thadani-Mulero M, Levy BP, Escuin D, Zhou XK, Gjyrezi A, Chanel-Vos C, Shen R, Tagawa ST, Bander NH, Nanus DM, Giannakakou P. Taxane-induced blockade to nuclear accumulation of the androgen receptor predicts clinical responses in metastatic prostate cancer. Cancer Res 2011;71 (18):6019–6029.

25. Gan L, Chen S, Wang Y, Watahiki A, Bohrer L, Sun Z, Wang Y, Huang H. Inhibition of the androgen receptor as a novel mechanism of taxol chemotherapy in prostate cancer. Cancer Res 2009;69(21):8386–8394.

26. Eigl BJ, Eggener SE, Baybik J, Ettinger S, Chi KN, Nelson C, Wang Z, Gleave ME. Timing is everything: Preclinical evidence supporting simultaneous rather than sequential chemohormonal therapy for prostate cancer. Clin Cancer Res 2005;11(13):4905–4911.

27. Chi KN, Chin JL, Winquist E, Klotz L, Saad F, Gleave ME. Multicenter phase II study of combined neoadjuvant docetaxel and hormone therapy before radical prostatectomy for patients with high risk localized prostate cancer. J Urol 2008;180(2):565–570.

28. Goodin S, Medina P, Capanna T, Shih WJ, Abraham S, Winnie J, Doyle-Lindrud S, Todd M, DiPaola RS. Effect of docetaxel in patients with hormone-dependent prostate-specific antigen progression after local therapy for prostate cancer. J Clin Oncol 2005;23(15):3352–3357.

29. Taplin ME, Xie W, Bubley GJ, Ernstoff MS, Walsh W, Morganstern DE, Regan MM. Docetaxel, estramustine, and 15-month androgen deprivation for men with prostate-specific antigen progression after definitive local therapy for prostate cancer. J Clin Oncol 2006;24(34):5408–5413.

30. Amato RJ, Teh BS, Henary H, Khan M, Saxena S. A retrospective review of combination chemohormonal therapy as initial treatment for locally advanced or metastatic adenocarcinoma of the prostate. Urol Oncol 2009;27(2):165–169.

Methods Mol Biol. 2013;1022:369-86. doi: 10.1007/978-1-62703-465-4_28.

Chapter 28

Tumor Targeting by a Carbohydrate Ligand-Mimicking Peptide

Shingo Hatakeyama, Toshiaki K. Shibata, Yuki Tobisawa, Chikara Ohyama, Kazuhiro Sugihara, and Michiko N. Fukuda

Abstract

Annexin A1 (Anxa1) is a highly specific surface marker of tumor vasculature. We used peptide-displaying phage technology to identify a carbohydrate ligand-mimicking 7-mer peptide, IFLLWQR (IF7), which can target Anxa1 in tumor vasculature. Here, we describe the binding activity of carbohydrate to Anxa1, Anxa1 to heparan sulfates, and the therapeutic potential of IF7 conjugated with anticancer drugs in tumor targeting.

Key words Annexin A1, Carbohydrate ligand-mimicking peptide, Lewis A, Heparan sulfate, Tumor targeting

1 Introduction

Although cancer malignancy is closely associated with carbohydrate structures found on tumor surfaces [1, 2], carbohydrate-based drug discovery has not been explored due to the technical difficulty involved in using chemically synthesizing complex carbohydrate structures. To improve this status, we employed peptide-displaying phage technology to identify peptides that act as carbohydrate ligands [3, 4]. During our experiments, we identified the IFLLWQR peptide (IF7) bound to annexin A1 (Anxa1) [5]. Anxa1 is a highly specific surface marker of tumor vasculature in several tumor types seen in both mice and humans [6]. Because IF7 is known to bind to Anxa1 fragments [5], we hypothesized that IF7 has potential to address the relationships between Anxa1 and carbohydrate in cancer, and it could serve as a tumor-specific drug delivery vector. We showed that IF7 mimicked the Lewis A oligosaccharide and Anxa1 bind to heparan sulfates on cell surface. Because it is well known that heparan sulfate regulates tumorigenesis, progression and metastasis [7, 8], and highly sulfated heparan

Inka Brockhausen (ed.), *Glycosyltransferases: Methods and Protocols*, Methods in Molecular Biology, vol. 1022, DOI 10.1007/978-1-62703-465-4_28, © Springer Science+Business Media New York 2013

sulfate were identified as preferential ligands of Anxa1 [9], the elongation of heparan sulfate by glycosyltransferases (EXT1/EXT2) has potential to play a key role for cancer biology though Anxa1 expression. In addition, we demonstrated that the specific Anxa1-binding peptide, IF7, is a highly efficient vector for targeted anticancer drug delivery in vivo for tumors in mice. IF7 conjugated with fluorescent Alexa Fluor 488 (IF7-A488) is known to bind to recombinant Anxa1 protein in a plate assay; in vivo imaging through a dorsal skinfold chamber window [10] showed accumulation of IF7-A488 in the tumors of mice. Moreover, tail vein injection of anticancer drugs (SN-38) conjugated with IF7 reduced tumor growth significantly. These results suggest that IF7 serves as an efficient drug delivery vector by targeting Anxa1 expressed on the surface of tumor vasculature. In this chapter we describe assays to analyze the binding activity of carbohydrate to Anxa1 and how to assess the therapeutic potential of IF7 conjugated with anticancer drugs in tumor targeting in mice.

2 Materials

2.1 Carbohydrate Binding Assays

1. Anxa1-His_6 stock solution: Full-length cDNA encoding Anxa1 was obtained from Invitrogen (Grand Island, NY, USA) and subcloned into the pET29a vector (Novagen, EMD Millipore Corp., Billerica, MA, USA) to produce an IF7-His_6 fusion protein. Recombinant proteins were purified by Ni+ affinity chromatography.
2. Superblock (10 %) (Takara Bio Company, Tokyo, JAPAN).
3. 96 well plates (Greiner bio-one North America Inc., Monroe, NC, USA).
4. 384 well plates (Greiner).
5. Blocking solution: 50 mM Tris–HCl buffer, pH 7.4 containing 0.15 M NaCl and 1 % bovine serum albumin.
6. Synthetic carbohydrates conjugated with biotinylated polyacrylamide (PAA) (Glycotech, Rockville, MD, USA).
7. TBSC solution: TBS containing 1 mM $CaCl_2$.
8. Peroxidase-conjugated streptavidin (Invitrogen, Grand Island, NY, USA).
9. Peroxidase substrate ABTS (Pierce, Rockford, IL, USA).
10. ELISA plate reader (Molecular Devices, Sunnyvale, CA, USA).
11. Peptides are synthesized by GenScript (Piscataway, NJ, USA). RQWLLFI peptide (RQ7) was used as a control as it has a sequence, which is reverse to that of IF7. To improve the solubility of the compounds, two arginine residues are added after the cysteine on IF7 and RQ7 to create IFLLWQR-C-RR [IF7(RR)] and RQWLLFI-C-RR [RQ7(RR)], respectively.

2.2 Anxa1 Binding to Heparan Sulfates

1. Mouse F2 cells, DMEM medium with 10 % fetal bovine serum (FBS) (Invitrogen, Grand Island, NY, USA).
2. 24-well dishes (Greiner).
3. Heparitinase (Seikagaku, Tokyo, Japan).
4. Bovine serum albumin (BSA), phosphate buffered saline (PBS).
5. Cell dissociation solution (EMD Millipore).
6. Anti-heparan sulfate antibody (10E4 clone, Seikagaku Corporation).
7. Rabbit anti-Anxa1 polyclonal antibodies (Invitrogen).
8. Alexa 647 conjugated anti-mouse IgM (Invitrogen).
9. Alexa 488 conjugated anti-rabbit IgG (Invitrogen).
10. FACS caliber (BD Biosciences pharmingen, San Diego, CA, USA).

2.3 IF7 And RQ7 Peptide Conjugation with Alexa Fluor 488 and an Anticancer Drug (SN-38)

1. Peptides: Peptides IF7, IF7(RR), RQ7, and RQ7(RR) were chemically synthesized as a custom order (GenScript, Piscataway, NJ, USA).
2. Solutions: Alexa Fluor 488 C5-maleimide (Invitrogen), SN-38 (Yakult Honsha, Tokyo, Japan), dimethylformamide (DMF), acetonitrile, trifluoroacetic acid (TFA), tranexamic acid, succinimidyl-4-(*N*-maleimidomethyl) cyclohexane-1-carboxylate (SMCC) (Pierce Biotechnology Inc. Rockford, IL, USA), dichloromethane (DCM), methanol, 0.1 M NaCl, 1 M Na-phosphate buffer pH 6.5, methyl tert-butyl ether (MTBE), O-(1H-6-chlorobenzotriazole-1-yl)-1, 1, 3, 3-tetramethyluronium (TCTU, Sigma-Aldrich, St. Louis, MA, USA), *N*-methyl pyrrolidone (NMP), *N,N-diisopropylethylamine* (DIPEA).
3. HPLC (Shimadzu LC-10 AD, Shimadzu Precision Instruments, Torrance, CA, USA) equipped with a C18 reverse-phase column (10 × 150 mm).
4. ESI, MALDI-TOF mass spectrometer (Waters, Micromass ZQ 2000) with MASSLYNX ver. 3.5 (Waters Corp., Milford, MA, USA).

2.4 Dorsal Skinfold Chamber Window

1. LLC cells (cultured in DME high glucose medium containing 10 % fetal bovine serum).
2. Athymic nude mice (aged 8–10 weeks, female, Balb/c) (*see* **Note 1**).
3. Anesthesia: 1.25 % 2,2,2-tribromoethanol (Sigma-Aldrich), syringes (1 mL), 26G needle, 70 % alcohol for disinfection, sterile surgical instruments [4–0 nylon strings, scissors, forceps, suture needle (size 20), and needle holder], and rubber gloves.
4. Special mounting stage: a handmade stage for holding a mouse (made from laboratory tubes or plastic instruments).

5. Dorsal skinfold chamber: Small dorsal kit (APJ Trading Co, Inc, Ventura, CA, USA), sterile coverslips (12 mm microscope glass cover, round).
6. Microscope and camera: Zeiss Axioplan fluorescence microscope and a digital camera system (DP70 and DP controller, Olympus, Centre Valley, PA, USA).
7. Antibody for inhibition assay: rabbit anti-Anxa1 antibody (N-19, Santa Cruz) and 28G syringes for tail vein injection.
8. 30G 1/2 needle, Silastic Lab tubing (0.012 × 0.025 in.) (VWR International, West Chester, PA, USA).
9. Signal intensity measurement: Image J (NIH, Bethesda, MD, USA).
10. DAPI stain (Vector laboratories, Burlingame, CA, USA).

2.5 Generation of Luciferase-Expressing HCT116-Luc Cells

1. HCT116 cells (cultured in DME high glucose medium containing 10 % fetal bovine serum) (Invitrogen).
2. Lentiviral plasmid vector CSII-Luc (constructed by Dr. Nikunj Somia, University of Minnesota, and provided by Dr. Renate Konig of Sanford-Burnham Medical Research Institute, La Jolla, CA, USA).

2.6 HCT116-Luc Tumor Monitoring by Luciferase Assay

1. Lewis lung carcinoma (LLC) and human colon carcinoma (HCT116) cells.
2. PBS, trypsin, DME medium, Matrigel (Becton-Dickinson, San Diego, CA, USA).
3. Athymic nude mice (aged 8–10 weeks, female, Balb/c).
4. Luciferin, isoflurane gas, Xenogen IVIS 200 imager (Caliper Life Sciences, Hopkinton, MA, USA).

3 Methods

3.1 Carbohydrate Binding Assay to Anxa1-His$_6$ Protein

1. Dilute Anxa1-His$_6$ stock solution (10 mg/mL, 63 μL) with 1 mL water.
2. Add 50 μL diluted Anxa1-His solution to 384-wells plate (31.25 ng/well) at 4 °C for 30 min.
3. Wash wells with water and block with 10 % superblock without Tween20. Anxa1-His$_6$ protein was coated on 96 wells plastic plate.
4. Each well is blocked with 50 mM Tris–HCl buffer, pH 7.4, containing 0.15 M NaCl (TBS) and 1 % bovine serum albumin.
5. Each synthetic carbohydrate conjugated with biotinylated polyacrylamide (PAA) is dissolved in TBS containing 1 mM $CaCl_2$ (TBSC), and is reacted with Anxa1-His$_{6\ at}$ room temperature for 15 min.

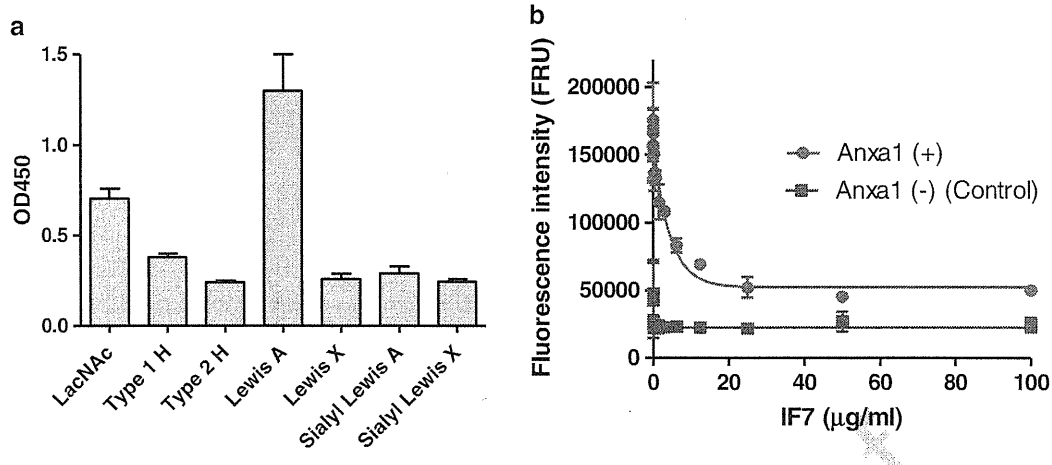

Fig. 1 Binding assay of carbohydrate antigens to Anxa1. (**a**) Binding of carbohydrate antigens conjugated to biotinylated polyacrylamide (PAA) with Anxa1-His protein. Recombinant Anxa1-His protein was coated on plastic wells and the biotinylated PAA-carbohydrate was added to the wells. *LacNAc*, Galβ1→4GlcNAcβ1→ PAA; *Type 1H*, Fucα1→2Galβ1→3GlcNAcβ1→PAA; *Type 2H*, Fucα1→2Galβ1→4GlcNAcβ1→PAA; *Lewis A*, Galβ1→3(Fucα1→4)GlcNAcβ1→PAA; *Lewis X*, Galβ1→4(Fucα1→3)GlcNAcβ1→PAA; *Sialyl Lewis A*, NeuNAcα2→3Galβ1→3(Fucα1→4)GlcNAcβ1→PAA; *Sialyl Lewis X*, NeuNAcα2→3Galβ1→4(Fucα1→3) GlcNAcβ1→PAA. (**b**) IF7C inhibition of FITC-Lewis A-PAA binding to Anxa1-His protein. Effect of IF7 (*red*) and control (*blue*) on binding of FITC-labeled polyacrylamide-Lewis A oligosaccharide to Anxa1-His protein

6. Wells are washed with TBSC, bound with peroxidase-conjugated streptavidin, and reacted with peroxidase substrate ABTS and read by an ELISA plate reader.
7. Analysis is performed in duplicate determinations. Error bars represent range (Fig. 1a). These data suggested strong candidate for anxa1 was Lewis A oligosaccharide. Wells coated with GST-His showed absorbance less than 0.113 (data not shown).

3.2 IF7C Inhibition of FITC-Lewis A-PAA Binding to Anxa1-His Protein

1. Dilute Anxa1-His_6 stock solution (10 mg/mL, 63 μL) with 1 mL water.
2. Add 50 μL diluted Anxa1-His solution to 384-wells plate (31.25 ng/well) at 4 °C for 30 min.
3. Wash wells with water and block with 10 % superblock without Tween 20.
4. Dilute 25 μL IF7C in 10 % superblock/TBSC.
5. Add 25 μL FITC-LeA-PAA (2 μg/mL) in 10 % superblock/TBSC.
6. Incubate at room temperature for 15 min.
7. Wash wells with TBSC three times and read fluorescence by plate reader (Fig. 1b). The data shown in Fig. 1b suggest that FITC-labeled polyacrylamide-Lewis A oligosaccharide binding was inhibited by the IF7 peptide.

3.3 Anxa1 Binds to Heparan Sulfates on Cell Surface

Because heparan sulfate regulates tumorigenesis, progression and metastasis [7, 8], and highly sulfated heparan sulfates were identified as preferential ligands of Anxa1 [9], the relationship between Anxa1 and heparan sulfate is determined in F2 cells.

1. F2 cells are cultured in 24-well dishes (10 % FBS-DMEM).
2. Exchange the medium to serum-free DMEM before heparitinase digestion.
3. 1 mU heparitinase is added in the wells. (BSA is used for control experiments).
4. Twenty-four hours after digestion, cells are dissociated by the cell dissociation solution.
5. The cells are washed twice with PBS.
6. The cells are reacted by anti-heparan sulfate (10E4 clone) and rabbit anti-Anxa1 antibody for 1 h on ice.
7. After washing with PBS, the cells are reacted with Alexa 647 conjugated anti-mouse IgM and Alexa 488 conjugated anti-Rabbit IgG for 1 h on ice.
8. The cells are washed twice with PBS and sequentially filtered. Cell surface Anxa1 and heparan sulfate are analyzed by FACS caliber (Fig. 2a, b) (*see* **Note 2**).

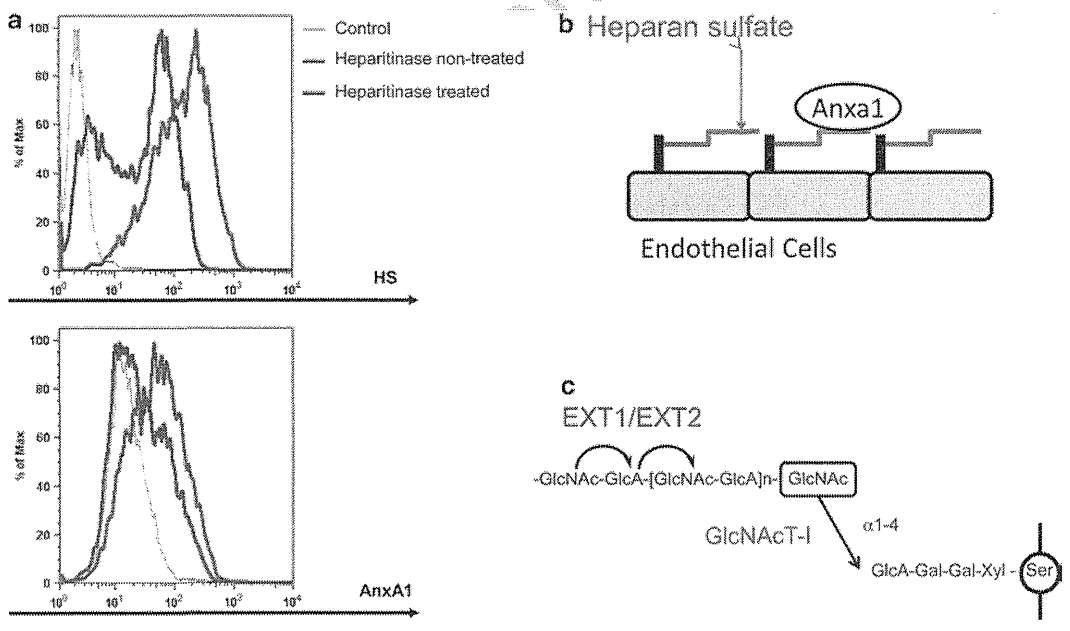

Fig. 2 Binding assay of Anxa1 to heparan sulfates on cell surface. Cell surface Anxa1 and heparan sulfate were analyzed by FACS caliber (**a**). After heparitinase digestion, the amount of cell surface heparan sulfate and Anxa1 were decreased. These data suggested the interaction between Anxa1 and heparan sulfate on cell surface (**b**), and the elongation of heparan sulfate by glycosyltransferases (EXT1/EXT2) potentially plays a key role for cancer biology (**c**)

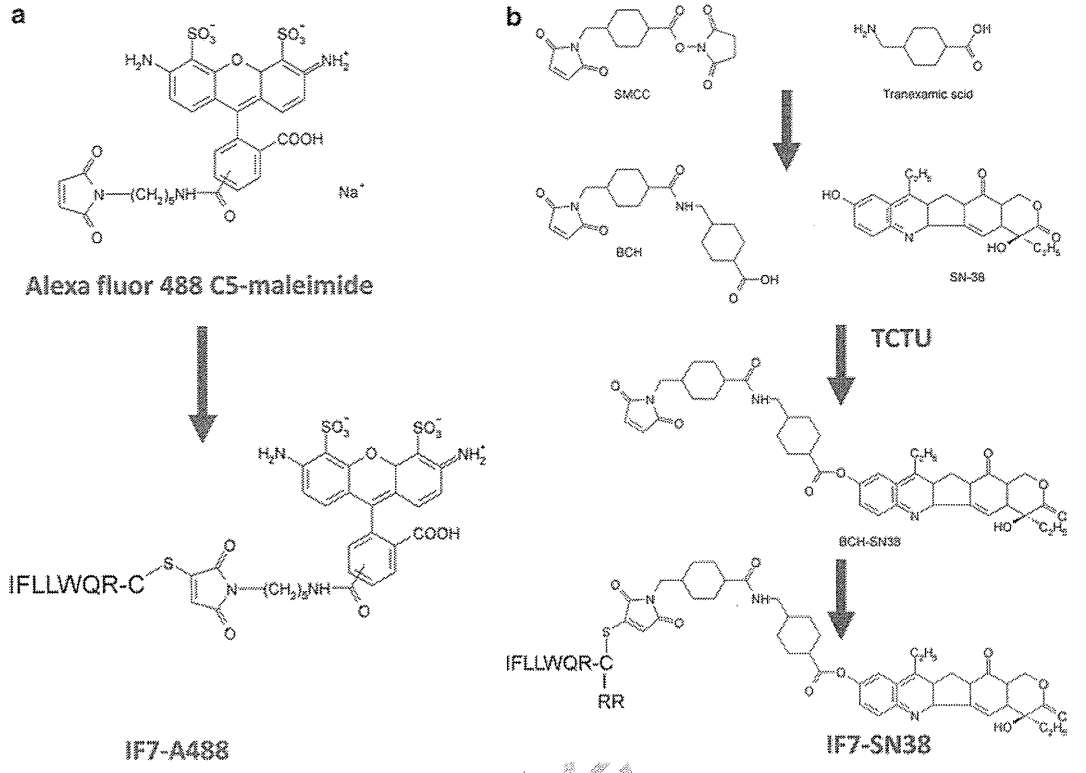

Fig. 3 IF7 peptide conjugation with Alexa Fluor 488 C5-maleimide (**a**) and IF7(RR) peptide conjugation with SN-38 (**b**). This figure shows a schematic diagram illustrating the conjugation of peptide with Alexa Fluor 488 C-5 maleimide (**a**) and a schematic diagram illustrating the conjugation of peptide with SN-38 (**b**)

3.4 IF7 Peptide Conjugation with Fluorescent Alexa 488

1. IF7 peptide (1 mg) is dissolved in DMF (0.4 mL), mixed with Alexa 488 (dissolved in 0.4 mL DMF), and incubated at room temperature for 4 h.
2. Water (2 mL) is added to the mixture and incubated at room temperature for 20 h.
3. The IF7-A488 product is purified by HPLC equipped with a C18 reverse-phase column (10 × 150 mm) using a linear gradient elution with 30–60 % acetonitrile in water containing 0.01 % TFA for 10 min at a flow rate of 2.5 mL/min.
4. The structure of the purified compound is validated by ESI mass spectrometry (Fig. 3a).

3.5 IF7 Peptide Conjugation with an Anticancer Drug (SN-38)

Peptide modification is performed in conjugation with SN-38 according to the method described by Meyer-Losic et al. [11]. Because the conjugated product (IF7-SN38) is poorly soluble in an aqueous solution, two arginine residues are added after the cysteine on IF7 to create IFLLWQR-C-RR [IF7(RR)], which thereby increased conjugate solubility.

1. Tranexamic acid (500 mg) is dissolved in water (12.5 mL), and pH adjusted by adding 1 mL 1 M Na-phosphate buffer pH 6.5.
2. SMCC (1 g) is dissolved in a mixture of acetonitrile (22 mL) and water (5.5 mL).
3. The tranexamic acid solution is then added to the SMCC solution, and the final mixture is incubated at 45 °C for 2 h.
4. Twenty milliliters of 2:1 (v/v) mixture of dichloromethane (DCM)–methanol and 60 mL DCM are added to the reaction mixture, and the organic phase is washed with water (20 mL) containing 0.1 M NaCl.
5. After removing the upper water phase, the organic phase is washed twice with water (5 mL), and evaporated using a rotary evaporator.
6. The dried material is dissolved in 9 mL of DCM–methanol (2:1) and methyl tert-butyl ether (40 mL), and left overnight at −20 °C.
7. The white precipitate 4-{4-[(*N*-maleimidomethyl)cyclohexanecarboxamido] methyl} cyclohexane-1-carboxylic acid linker (BCH) was collected by centrifugation.
8. The structure of BCH is confirmed by MALDI-TOF mass spectrometry.
9. TCTU (310 mg) is dissolved in NMP (5 mL) and DIPEA (540 μL) and added to the mixture.
10. BCH (580 mg) dissolved in NMP (5 mL) and SN-38 (450 mg) dissolved in NMP (5 mL) is then added to the mixture. The final mixture is allowed to react at room temperature for 4 h.
11. The product, BCH-SN38 conjugate, is dissolved in DCM (80 mL), which is washed thrice with 5 % aqueous citric acid and once with water.
12. The product is concentrated to 2–3 mL by a rotary evaporation, transferred to a tube to which MTBE (10 mL) is added, and precipitated at −20 °C to form a yellow precipitate.
13. BCH-SN38 (150 mg) is dissolved in DMF (1 mL) and mixed with IF7RR peptide (200 mg) dissolved in DMF (1 mL). The mixture is then incubated at 45 °C for 3 h.
14. Water (10 mL) is added to the mixture, which is then rotated at room temperature for 20 h.
15. DCM (30 mL) and 5 M NaCl (2 mL) are added to the mixture, which is then centrifuged.
16. The upper water phase is removed and the organic phase is washed thrice with water (10 mL each time).
17. IF7(RR)-BCH-SN38 forms a semi-solid interphase that is collected by decantation, suspended in water, and completely dried in vacuum.

18. Crude IF7(RR)-BCH-SN38 is dissolved in 50 % acetonitrile–water and purified by HPLC using a linear gradient elution with 50–70 % acetonitrile in water containing 0.01 % TFA over 20 min at a flow rate of 2.5 mL/min. The elution position (acetonitrile concentration) of each compound is as follows: SN-38 (50.3 %), BCH (53.5 %), BCH-SN38 (67.1 %), IF7 (48.2 %), and IF7(RR)-BCH-SN38 (59.7 %).
19. The structure of the purified compound is validated by mass spectrometry (Fig. 3b).

3.6 Surgical Preparation of the Dorsal Skinfold Chamber

The dorsal skinfold chamber is prepared according to the protocol described previously [12, 13]. We describe our protocol in brief:

1. Nude mice are anesthetized with a peritoneal injection of 1.25 % 2,2,2-tribromoethanol (25 μL/g) (*see* **Note 3**).
2. The skin on the back of each mouse is dried and disinfected with a 70 % alcohol-soaked swab (*see* **Note 4**).
3. A fold of the depilated dorsal skin parallel to the spine is then lifted up (Fig. 4a).
4. The rear of the titanium frame of the chamber is then attached to the fold on the right side of the mouse (Fig. 4b), and the mouse is temporarily fixed into position with string (Fig. 4c).
5. The mouse is then inverted (left side of the mouse facing the technician), and a resection line is marked on the skin (Fig. 4d).

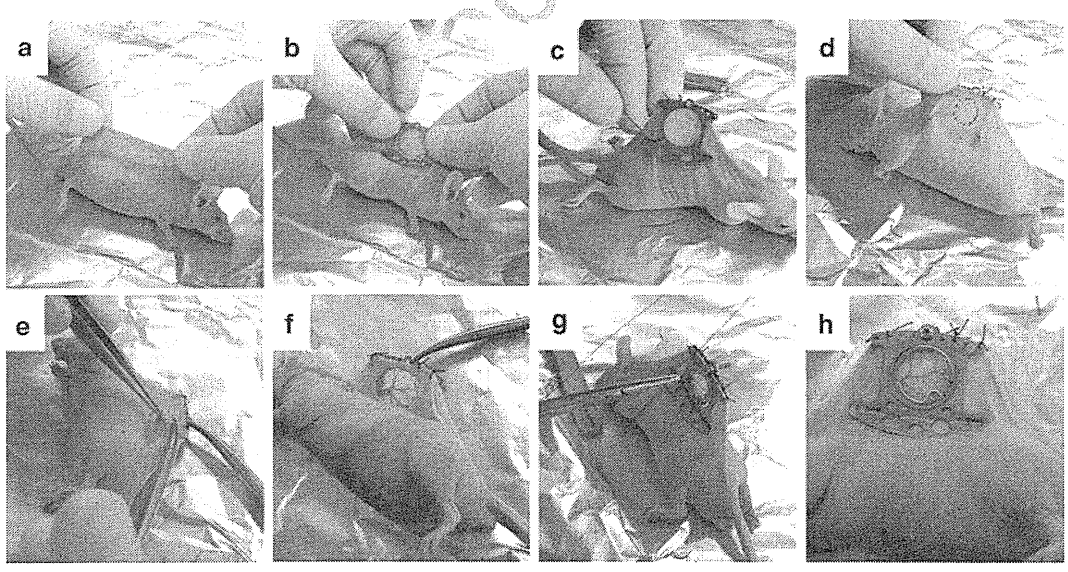

Fig. 4 Surgical preparation of the dorsal skinfold chamber. Lift up a fold of the depilated dorsal skin parallel to the spine (**a**). Place the rear part of the titanium frame of the chamber on the *right side* of the mouse (**b**), and temporarily fix it in place using string (**c**). Next, invert the mouse (*left side* of the mouse facing the technician) and mark the *resection line* (**d**). Remove the skin carefully with a pair of scissors (**e**, **f**). Place the front part of the titanium frame on the *left side* and temporarily fix it to the first frame with an upper screw and holding sutures (**g**). Hold the sandwiched skinfold together to spread out the skin and fix the edges in place using sutures (**h**)

6. The skin on the left side is then removed using a pair of scissors (Fig. 4e, f) (*see* **Note 5**).
7. The front of the titanium frame is then temporarily fixed in position, and attached to the first frame with an upper screw and holding sutures (Fig. 4g) (*see* **Note 6**).
8. Holding sutures are spread out and the edges of the sandwiched skinfold fixed in place (Fig. 4h) (*see* **Note 7**).
9. The mouse is then placed in its cage and observed until it regains consciousness. A waiting period of at least 3 days is needed before tumor implantation. The skinfold may became ischemic, and necrosis or edema occurs (*see* **Note 8**).

3.7 In Vivo Imaging in the Dorsal Skinfold Chamber Window

1. An LLC tumor is produced in a donor nude mouse by subcutaneous injection.
2. The donor mouse is then sacrificed and the LLC tumor removed under aseptic conditions using sterile surgical instruments (scissors and forceps). The LLC tumor is then placed in DMEM without serum (Fig. 5a).
3. After the tumor is removed from the donor mouse, the glass cover of the chamber window is opened and a small piece of tumor (<1 mm^3) is transplanted onto the dorsal skinfold of the recipient nude mouse (Fig. 5b) (*see* **Note 9**).

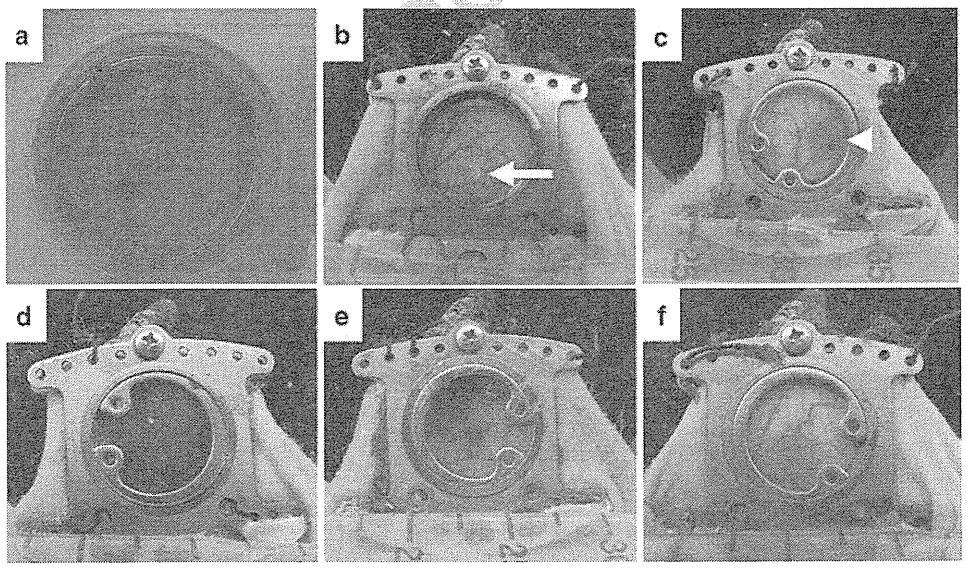

Fig. 5 Tumor transplantation from a donor mouse to the dorsal skinfold chamber. Remove a Lewis lung carcinoma (LLC) tumor produced in a donor nude mouse using subcutaneous injection and sterile techniques (**a**). Transplant a small piece of the tumor (<1 mm^3) into a dorsal skinfold chamber in a recipient nude mouse (aged 8–10 weeks, female, Balb/c) (**b**, *arrow*). Three days later, check the tumor (**c**, *arrowhead*). In some cases, bloody (**d**), edematous (**e**), or thick (**f**) tumors are observed in the skinfold chamber

4. The tumor is analyzed after 3 days (Fig. 5c). Bloody, edematous, or thick tumors are often observed due to the difficulty in creating a suitable tumor with sufficient tumor vasculature in the skinfold chamber (Fig. 5d–f, respectively).
5. The mouse is then anesthetized by peritoneal injection of 1.25 % 2,2,2-tribromoethanol (25 μL/g) and placed on the mounting stage.
6. An injection needle (30G 1/2) is then cut and connected to silastic tubing (0.012 × 0.025 in.). The other side of the needle is connected to a 26–28G needle and a 1 mL syringe filled with ultrapure water.
7. Once the mouse is placed on the mounting stage, the needle is positioned and a catheter is inserted into the tail vein (Fig. 6a, b) (*see* **Note 10**). If the technician successfully inserts the needle in the vein, back flow of blood is visible; patency is confirmed by administering 0.1–0.2 mL of the liquid in the syringe (*see* **Note 11**).
8. The tail and catheter are carefully taped to the holder (Fig. 6c, d), then the water-filled syringe is replaced with a peptide-filled syringe (IF7-A488 or RQ7-A488, 100 μL; 50 μM in 5 % glucose

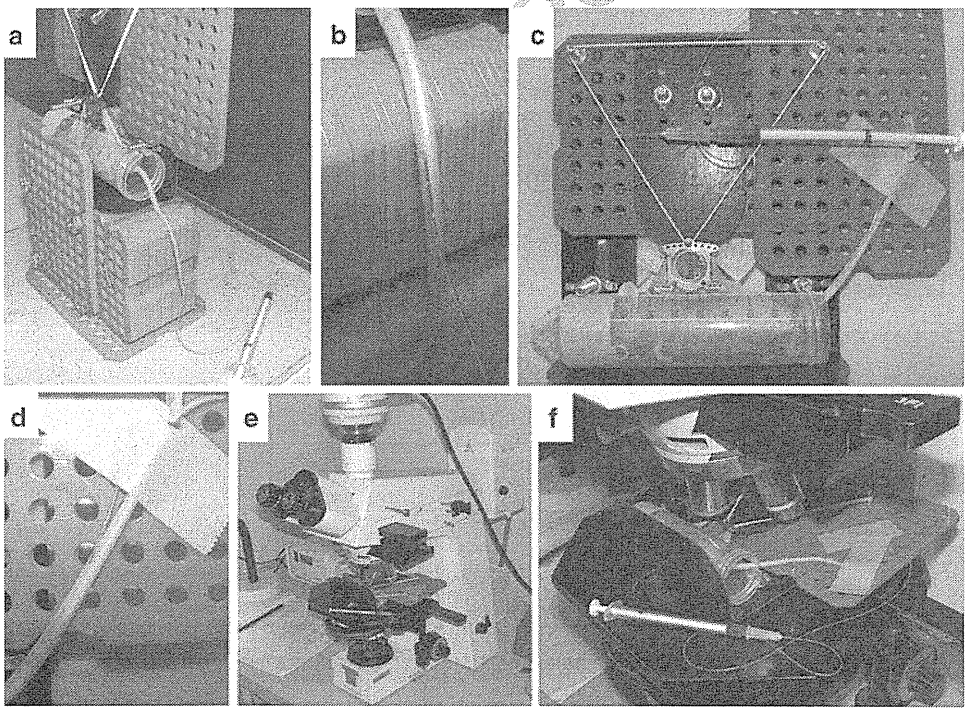

Fig. 6 The mounting stage, tail vein catheterization, and microscope settings. Insert the 30G 1/2 needle keeping the catheter in the tail vein (**a**, **b**). Tape the tail and the catheter to the holder very carefully (**c**, **d**). Next, exchange the water-filled syringe for a peptide-filled syringe (IF7-A488 or RQ7-A488, 100 μL; 50 μM in 5 % glucose solution) and place the chamber in a position for easy viewing by fluorescence microscope (**e**, **f**)

solution) and the skin chamber is assessed with the fluorescence microscope (Fig. 6e, f).

9. Tumor vasculature is initially checked by bright-field microscopy and then adjusted to zero point by fluorescence field (*see* **Note 12**).
10. IF7-A488 or RQ7-A488 is injected through the tail vein. Intravital Alexa 488 signals in the tumor are detected and recorded by a Zeiss Axioplan fluorescence microscope and a digital camera system with a quad magnification objective lens. Images are captured every 1 min from 0 to 10 min and every 5 min thereafter (Fig. 7a) (*see* **Note 13**). For the inhibition assays, 20 μg of rabbit anti-Anxa1 antibody (N-19) is injected 15 min prior to the IF7-A488 injection. Signal intensity in the tumor is measured from 0 to 40 min using Image J software. The intensity of 5–10 areas is measured and the mean calculated for each point (Fig. 7b).

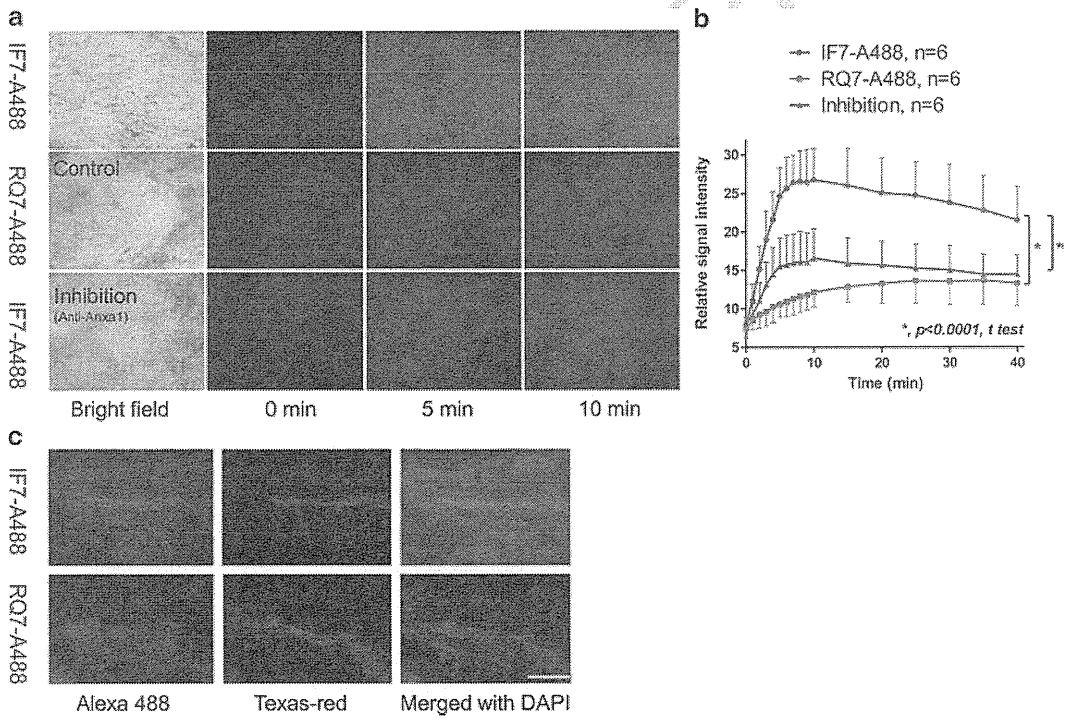

Fig. 7 In vivo imaging. When IF7-A488 was injected through the tail vein, fluorescence signals appeared in the tumor within 1 min of injection, reached a plateau after 9 min, and remained high for 40 min or until the experiment was terminated. By contrast, control peptide RQ7-A488 signals remained at background levels. When the anti-Anxa1 antibody was injected prior to IF7-A488 injection, fluorescence signals in the tumors were significantly reduced (**a**, **b**). Normal rabbit IgG (control IgG) did not alter the tumor targeting of IF7-A488 (data not shown). (**c**) Fluorescence micrographs of tumor sections 20 min after injection with IF7-A488 or RQ7-A488, coinjected with Texas-red conjugated tomato lectin. Shown are IF7-A488 or RQ7-A488 (*left*), Texas-red tomato lectin (*middle*), and the merge with DAPI nuclear staining (*right*) (scale bar; 50 μm)

11. After in vivo measurement, the tumor is isolated from the dorsal skin folder chamber, fixed with 4 % paraformaldehyde at room temperature for 15 min, immersed in Optimal Cutting Temperature (O.C.T) compound, and cryosectioned. Frozen sections are overlaid with Vectashield containing DAPI and examined under a Zeiss Axioplan fluorescence microscope (Fig. 7c).

3.8 Tumor Targeting Treatment Using IF7(RR)-SN38 for a Small Tumor

1. HCT116 cells are cultured in DME high glucose medium containing 10 % fetal bovine serum.
2. The lentiviral plasmid vector CSII-Luc and lentivirus is used to transfect HCT116 cells which are maintained as HCT116-Luc cells [14] (The lentiviral plasmid vector CSII-Luc constructed by Dr. Nikunj Somia of the University of Minnesota was provided by Dr. Renate Konig of the Sanford-Burnham Medical Research Institute).
3. HCT116-Luc cells are trypsinized and suspended in DME medium containing 1 mg/mL Matrigel placed on ice. Cell suspensions (50 μL) containing 5×10^5 cells are injected subcutaneously into 8–10-week-old female nu/nu mice.
4. After tumor injection, the mice are subjected to imaging for luciferase producing tumors; 100 μL of luciferin (30 mg/mL PBS) is injected into the peritoneal cavity of each mouse.
5. Mice are anesthetized under isoflurane gas (20 mL/min) supplemented with oxygen (1 L/min), and placed under a camera in a Xenogen IVIS 200 imager. Photons are measured (1–10 s) every 2–3 days.
6. Ten days later, the tumor-bearing mice are divided randomly into three groups and administered (1) 5 % glucose, (2) 0.81 μmol/kg (1.74 mg/kg) RQ7(RR)-SN38, or (3) 0.81 μmol/kg (1.74 mg/kg) IF7(RR)-SN38 on days 0 to 9 (10 times) (*see* **Note 14**, Fig. 8).

3.9 Tumor Targeting Treatment with IF7(RR)-SN38 for a Large Tumor

1. HCT116-Luc cells were injected subcutaneously into the dorsal flank of 8–10-week-old female nu/nu mice, and these were then subjected to imaging for luciferase producing tumors, as described previously.
2. Twenty-three days later, tumor-bearing mice were administered 6.5 μmol/kg (13.9 mg/kg) IF7(RR)-SN38. IF7(RR)-SN38 was administered on days 23–43 (20 times). Tumor size was dramatically reduced after IF7(RR)-SN38 injection (Fig. 9a, b). It is notable that the IF7-SN38 injections administered here contained 0.81 μmol/injection (1.74 mg/kg) or 6.5 μmol/kg (13.9 mg/kg), whereas the effective dose of SN-38 conjugated with a non-tumor vasculature targeting peptide was reported to be 95 mg/kg in a previous study [11] (Table 1).